



---

Year: 2016

---

## A method to measure sound transmission via the malleus-incus complex

Dobrev, Ivo ; Ihrle, Sebastian ; Rösli, Christof ; Gerig, Rahel ; Eiber, Albrecht ; Huber, Alexander M ;  
Sim, Jae Hoon

**Abstract:** **BACKGROUND:** The malleus-incus complex (MIC) plays a crucial role in the hearing process as it transforms and transmits acoustically-induced motion of the tympanic membrane, through the stapes, into the inner-ear. However, the transfer function of the MIC under physiologically-relevant acoustic stimulation is still under debate, especially due to insufficient quantitative data of the vibrational behavior of the MIC. This study focuses on the investigation of the sound transformation through the MIC, based on measurements of three-dimensional motions of the malleus and incus with a full six degrees of freedom (6 DOF). **METHODS:** The motion of the MIC was measured in two cadaveric human temporal bones with intact middle-ear structures excited via a loudspeaker embedded in an artificial ear canal, in the frequency range of 0.5-5 kHz. Three-dimensional (3D) shapes of the middle-ear ossicles were obtained by sequent micro-CT imaging, and an intrinsic frame based on the middle-ear anatomy was defined. All data were registered into the intrinsic frame, and rigid body motions of the malleus and incus were calculated with full six degrees of freedom. Then, the transfer function of the MIC, defined as velocity of the incus lenticular process relative to velocity of the malleus umbo, was obtained and analyzed. **RESULTS:** Based on the transfer function of the MIC, the motion of the lenticularis relative to the umbo reduces with frequency, particularly in the 2-5 kHz range. Analysis of the individual motion components of the transfer function indicates a predominant medial-lateral component at frequencies below 1 kHz, with low but considerable anterior-posterior and superior-inferior components that become prominent in the 2-5 kHz range. **CONCLUSION:** The transfer function of the human MIC, based on motion of the umbo and lenticularis, has been visualized and analyzed. While the magnitude of the transfer function decreases with frequency, its spatio-temporal complexity increases significantly.

DOI: <https://doi.org/10.1016/j.heares.2015.10.016>

Posted at the Zurich Open Repository and Archive, University of Zurich

ZORA URL: <https://doi.org/10.5167/uzh-117061>

Journal Article

Accepted Version



The following work is licensed under a Creative Commons: Attribution-NonCommercial-NoDerivatives 4.0 International (CC BY-NC-ND 4.0) License.

Originally published at:

Dobrev, Ivo; Ihrle, Sebastian; Rösli, Christof; Gerig, Rahel; Eiber, Albrecht; Huber, Alexander M; Sim, Jae Hoon (2016). A method to measure sound transmission via the malleus-incus complex. Hearing

research, 340:89-98.

DOI: <https://doi.org/10.1016/j.heares.2015.10.016>

# Accepted Manuscript

A method to measure sound transmission via the malleus-incus complex

Ivo Dovrev, Sebastian Ihrle, Christof Rösli, Rahel Gerig, Albrecht Eiber, Alexander M. Huber, Jae Hoon Sim



PII: S0378-5955(15)30095-2

DOI: [10.1016/j.heares.2015.10.016](https://doi.org/10.1016/j.heares.2015.10.016)

Reference: HEARES 7043

To appear in: *Hearing Research*

Received Date: 31 July 2015

Revised Date: 22 October 2015

Accepted Date: 29 October 2015

Please cite this article as: Dovrev, I., Ihrle, S., Rösli, C., Gerig, R., Eiber, A., Huber, A.M, Sim, J.H., A method to measure sound transmission via the malleus-incus complex, *Hearing Research* (2015), doi: 10.1016/j.heares.2015.10.016.

This is a PDF file of an unedited manuscript that has been accepted for publication. As a service to our customers we are providing this early version of the manuscript. The manuscript will undergo copyediting, typesetting, and review of the resulting proof before it is published in its final form. Please note that during the production process errors may be discovered which could affect the content, and all legal disclaimers that apply to the journal pertain.

1     **A method to measure sound transmission via the malleus-incus complex**

2

3 Ivo Dobrev<sup>1,\*</sup>, Sebastian Ihrle<sup>2</sup>, Christof Rösli<sup>1</sup>, Rahel Gerig<sup>1</sup>, Albrecht Eiber<sup>2</sup>,  
4 Alexander M Huber<sup>1</sup>, Jae Hoon Sim<sup>1</sup>

5

6 <sup>1</sup>University Hospital Zurich, University of Zurich, Zurich, Switzerland

7

8 <sup>2</sup>University of Stuttgart, Stuttgart, Germany

9

10 \*Corresponding author: Otolaryngology, Head and Neck Surgery, University Hospital Zurich,

11 University of Zurich, Frauenklinikstrasse 24, 8091 Zurich, Switzerland; ivo.dobrev@uzh.ch

12

13

14 For submission to Hearing Research as part of the proceedings of the MEMRO 2015 meeting,

15 Aalborg, Denmark, July 1–5, 2015

16 **Abstract**

17 **Background:** The malleus-incus complex (MIC) plays a crucial role in the hearing process as  
18 it transforms and transmits acoustically-induced motion of the tympanic membrane, through  
19 the stapes, into the inner-ear. However, the transfer function of the MIC under  
20 physiologically-relevant acoustic stimulation is still under debate, especially due to  
21 insufficient quantitative data of the vibrational behavior of the MIC. This study focuses on the  
22 investigation of the sound transformation through the MIC, based on measurements of three-  
23 dimensional motions of the malleus and incus with a full six degrees of freedom (6 DOF).

24 **Methods:** The motion of the MIC was measured in two cadaveric human temporal bones with  
25 intact middle-ear structures excited via a loud speaker embedded in an artificial ear canal, in  
26 the frequency range of 0.5-5 kHz. Three-dimensional (3D) shapes of the middle-ear ossicles  
27 were obtained by sequent micro-CT imaging, and an intrinsic frame based on the middle-ear  
28 anatomy was defined. All data were registered into the intrinsic frame, and rigid body motions  
29 of the malleus and incus were calculated with full six degrees of freedom. Then, the transfer  
30 function of the MIC, defined as velocity of the incus lenticular process relative to velocity of  
31 the malleus umbo, was obtained and analyzed.

32 **Results:** Based on the transfer function of the MIC, the motion of the lenticularis relative to  
33 the umbo reduces with frequency, particularly in the 2-5 kHz range. Analysis of the individual  
34 motion components of the transfer function indicates a predominant medial-lateral component  
35 at frequencies below 1 kHz, with low but considerable anterior-posterior and superior-inferior  
36 components that become prominent in the 2-5 kHz range.

37 **Conclusion:** The transfer function of the human MIC, based on motion of the umbo and  
38 lenticularis, has been visualized and analyzed. While the magnitude of the transfer function  
39 decreases with frequency, its spatio-temporal complexity increases significantly.

40

41

42 **Keywords:** Malleus-Incus complex, 3D Laser Doppler Vibrometer, rigid-body motion,  
43 human middle-ear, 3D transfer function, incudo-malleolar joint; micro-CT

44

45 **Abbreviations:** ASTM - American Society for Testing and Materials; DOF - degree(s) of  
46 freedom; IMJ - incudo-malleolar joint; ISJ - incudo-stapedial joint; LDV - laser Doppler  
47 vibrometry; LPI - lenticular process of the incus; MIC - malleus-incus complex; RBM - rigid  
48 body motion; SNR - signal-to-noise ratio; TB - temporal bone; 3D - three dimensional

49

## 50 **1. Introduction**

51 Acoustically-induced motions of the tympanic membrane cause three-dimensional  
52 vibrations of the middle-ear ossicles. Sophisticated techniques are needed to measure the  
53 vibrational motions of the middle-ear ossicles because the amplitude of the ossicular vibration  
54 is on a nanometer scale. Previous investigations (Decraemer et al. 1999; Puria 2003) have  
55 revealed that the Laser Doppler Vibrometer (LDV) provides sufficiently sensitive, reliable  
56 and accurate measurements for determining vibration modes of the middle-ear bones.

57 Considering motion of each of the middle-ear ossicles (i.e., the malleus, incus, and  
58 stapes) as a rigid body motion under physiologically-relevant acoustical stimulation, three-  
59 dimensional (3D) motions of each ossicle have six degrees of freedom (DOF), consisting of  
60 three translations and three rotations, and thereby the ossicular motion of the middle-ear  
61 bones can be described in a common reference frame. From a theory of classical dynamics,  
62 the six rigid-body motion (RBM) components can be determined when the spatial motion  
63 components and coordinates of more than three non-co-linear points on the rigid body are  
64 known. Decraemer et al. (1994) presented a method for determining three translational  
65 components at a specific point on the middle-ear bones from measurements using a one-  
66 dimensional (1D) LDV. They mounted temporal bones on two stacked goniometers and  
67 measured velocities using a laser Doppler vibrometer from several different angles, which  
68 were provided by rotations of the two goniometers. Recent developments and  
69 commercialization of 3D LDV systems with three built-in laser beams, oriented at three  
70 independent measurement angles, allow for accurate and simultaneous measurements of all  
71 three translational components at a measurement point.

72 In the previous studies, spatial motion of the stapes was measured for humans (Hato et  
73 al. 2003; Sim et al. 2010a) and for guinea pigs (Sim et al. 2010b) with an assumption that in-  
74 plane motion of the stapes along the footplate plane is restricted due to anatomy of the annular  
75 ligaments, and thus motion of the stapes has only three dominant spatial motion components.  
76 Lauxmann et al. (2012) measured motion of the human stapes with the full six DOF, but in  
77 their measurements the cochlea was drained, which may have significantly changed the  
78 physiological response of the samples. They measured 3-D motion components at nine points  
79 on the medial side of the footplate using a 3-D LDV system, and reconstructed the six rigid-  
80 body motion components from the measurement. Decraemer et al. (2007) also measured  
81 motion of the gerbil stapes with the full six degrees of freedom. In their study, the  
82 measurement points were aligned at the center of the rotations of the goniometers, and thus

83 the location of the measured points could be maintained during the rotations by the  
84 goniometers.

85 While spatial motion of the stapes has been measured in several previous studies,  
86 measurements of spatial motion of the malleus or the incus have involved technical  
87 difficulties. First, the spatial motions of each of the malleus and incus are expected to have  
88 full six degrees of freedom involving their relative motion at the incudo-malleal joint (IMJ),  
89 and thus simplification of the spatial motion is not applicable. Second, surgical opening for  
90 access to the malleus and incus is limited because the malleus-incus complex is suspended by  
91 several ligaments and tendons and those must not be damaged to measure physiological  
92 motion of the malleus-incus complex. Such difficulty in surgical opening becomes more  
93 serious with the 3D LDV system because access of the three beams from the 3D LDV system  
94 requires wider surgical opening. Sim et al. (2004) measured spatial motion of the malleus-  
95 incus complex with full six degrees of freedom, but in their measurements, the malleus-incus  
96 complex was isolated, with the stapes and extraneous bones removed, to obtain sufficient  
97 access of the laser beam of the LDV system to the malleus and the incus. This study found  
98 significant relevant motion between the malleus and incus that increased with frequency.  
99 Decraemer et al. (2014) measured the spatial motion of the MIC in living gerbils and found a  
100 frequency dependence on the direction of the instantaneous rotational axis (hinged motion)  
101 between the malleus and incus. In this study they removed circular pars flaccida for access the  
102 LDV laser beam. In addition, in their measurements, sophisticated measurement setup and  
103 procedures with a custom-made positioning system were needed with use of a 1D LDV  
104 system.

105 In this study, a method to measure and determine spatial motions of the malleus and  
106 the incus with the full six DOF using a 3D LDV system is introduced, and the method is  
107 applied to two human cadaveric temporal bones. The 3D LDV system is positioned by several  
108 different angles with respect to the specimen due to limited access of the laser beam to the  
109 malleus and the incus. To identify spatial coordinates of the measurement points on the  
110 ossicles with different orientations of the 3D LDV system, spatial registration techniques  
111 using micro-CT imaging are used.

112

## 113 2. Methods

### 114 2.1. Temporal Bone Preparation

115 A fresh cadaveric temporal bone (TB), TB1, and a frozen TB, TB2, were used for this  
116 study. The fresh TB was harvested within 24 hours after death and was preserved in  
117 thiomersal 0.1 % ( $C_9H_9HgNaO_2S$ ) solution at 4° C. The frozen TB was also harvested within  
118 24 hours after death and was frozen immediately. The use of human TBs in this study was  
119 approved by the Ethical Committee of Zurich (KEK-ZH-Nr. 2012-0007).

120 A canal-wall-up mastoidectomy including posterior tympanotomy and a wide  
121 epitympanectomy were performed subsequently to expose the malleus-incus complex as  
122 much as possible. After the surgical opening, the superior part of the malleus head and incus  
123 body, the manubrium of the malleus, and the long process of the incus were exposed. The  
124 intact tympanic membrane (TM) was confirmed by microscopic view, and all suspensory  
125 attachments to the middle-ear ossicles, which include ligaments and tendons, were left intact,  
126 during the preparation. The external ear canal was drilled down near the tympanic membrane  
127 for stable positioning of an artificial ear canal (AEC) without air leakage. The AEC allowed  
128 to for the control of the volume and distance between the microphone probe and the TM  
129 center, maintained at 5ml and approximately 5 mm, respectively. (Sim et al., 2010, 2012;  
130 Lauxmann et al., 2012; Gerig et al. 2015).

131 Several custom-made markers were glued on the peripheral bones as references for  
132 identification of the LDV measurement frame (see Section 2.3), and were held in position  
133 during the measurements. The marker consists of a silica glass tube (diameter of 0.3 mm and  
134 length of 1-3mm) and a copper wire (diameter of 0.05 mm) embedded in the silica glass tube.

### 136 2.2 Measurement of vibration of the malleus and incus

137 Figure 1 illustrates the measurement setup schematically. The major components of  
138 the setup are: 1) a three-dimensional Laser Doppler Vibrometry (3D LDV, CLV-3000, CLV-  
139 3D, Polytec, Germany) system for measurements of the motion of the ossicles; 2) speaker and  
140 microphone for application of controlled acoustic stimuli; 3) mechanical positioners for  
141 control of the relative position between the sample and the 3D LDV.

142 The TBs were mounted on a custom-made three-axis gimbal stage allowing for control  
143 over the viewing angle to the sample. The position of the 3D LDV was controlled via a 3-axis  
144 positioner consisting of three electrically-driven micro-positioning translation stages (PI  
145 Physik Instrumente M-126.CG1/DG1, Karlsruhe, Germany) mounted on a support frame. The  
146 position of the 3D LDV laser spot was identified by displacement encoders integrated into the

147 translational stages, with a bidirectional repeatability of 2.5  $\mu\text{m}$ . The control of the  
148 translational stages and recording of the position of the 3D LDV system from the  
149 displacement encoders was done in real-time by dSPACE (Paderborn, Germany). A USB  
150 microscopic camera (Digimicro 1.3, DNT, Germany) was attached to the measurement head  
151 of the 3D LDV system by means of a reflective prism (mirror) for visual observation of the  
152 laser spot on the surface of the malleus and incus (Lauermann et al. 2012).

153 A loudspeaker (ER-2, Etymotic Research, USA) and a microphone (ER-14C,  
154 Etymotic Research, USA) were placed in the AEC, in order to generate the sound stimuli and  
155 monitor the sound pressure levels inside the AEC. Two sets of multi-frequency harmonic  
156 signals (0.5-2 kHz and 2-5 kHz) were generated by a function generator embedded in the  
157 dSPACE data acquisition system and were delivered to the loudspeaker via an amplifier. To  
158 reduce the crest factor of the resulting signal and prevent the peak amplitude of the resulting  
159 signal from exceeding the maximum allowable voltage to the loudspeaker (2 Volts), the  
160 phases of the sinusoidal components were optimized using a Schroeder multi-sine phase  
161 distribution. (Gatto et al. 2010). The frequency steps were 12.5 Hz through the stimulation  
162 frequency range. With the two sets of the multi-frequency harmonic signals, AEC pressure  
163 levels of 80-95 dB SPL were obtained.

164 With the acoustic stimulation, spatial motion components (i.e., XYZ components) of  
165 each measurement point were measured by the 3D LDV system. The measured signals were  
166 digitized with a sampling frequency of 51.2 kHz after filtering with VBF 44 filter modules  
167 (Kemo, Dartford, United Kingdom) with the low-pass filter cut-off set at 12.5 kHz. The  
168 recording of the data was done through eight signal channels in dSPACE, which consists of  
169 six channels from the 3D-LDV unit (three raw signals and three Cartesian signals obtained  
170 from the build in geometry module), a channel for the pressure in the ear canal, and a channel  
171 for the excitation signal. The measurements at each point were repeated 30 times (30  
172 measurement blocks), and were averaged. All the measurement procedures were controlled by  
173 an external computer using a custom-made algorithm.

174 The measurements of the vibrational motion were performed at 6-8 points on the  
175 malleus, and 8-10 points on the incus. The measurement points were located on the superior  
176 part of the malleus head and incus body, the manubrium of the malleus, and the long process  
177 of the incus, and access of the laser beams from the 3D LDV system could be obtained with  
178 several different orientations of the TBs (three orientations for TB1 and two orientations for  
179 TB2).

180 During the velocity measurement,  $XY$  coordinates of the measurement points in the 3D  
181 LDV measurement frame ( $XYZ$  coordinate system), in which the  $Z$ -axis along the laser beam  
182 (positive direction of the  $Z$ -axis toward the LDV head) and the  $XY$  plane is perpendicular to  
183 the laser beam, were recorded by the displacement encoders of the translational stages. The  
184  $XY$  coordinates of one end of the markers in the 3D LDV measurement frame were also  
185 recorded. The recorded  $XY$  coordinates of the measurement points and markers were used for  
186 identification of the 3D LDV measurement frame and the measurement points (see Section  
187 2.3).

188

## 189 **2.3 Frame Registration**

### 190 **2.3.1 Micro-CT Imaging**

191 After the velocity measurement, the TB with the markers (see Section 2.1 for details)  
192 was scanned by a high-resolution micro-CT scanner (vivaCT 40, SCANCO Medial AG,  
193 Switzerland). The resolution was set to 15  $\mu\text{m}$ , and the photon energy level was set to 55 keV  
194 (Sim and Puria 2008). The 3-D volumes of the malleus, the incus, the stapes, and the markers  
195 were reconstructed from the micro-CT slice images. The copper wires in the markers were  
196 clearly visible and distinguishable from bones in the micro-CT images because the copper had  
197 much larger x-ray attenuation than the bones and soft tissues (Sim et al. 2009, 2012).

198

### 199 **2.3.2 Intrinsic Frame (anatomical frame)**

200 The  $xyz$  coordinate system of the intrinsic frame (i.e., anatomical frame) was defined  
201 based on the geometry of the medial surface of the stapes footplate (Sim et al. 2013) and the  
202 center of mass of the malleus-incus complex (Note that the  $xyz$  coordinate system is attributed  
203 to the intrinsic frame whereas the  $XYZ$  coordinate system is attributed to the LDV  
204 measurement frame). First, in order to determine the directions of the intrinsic frame axes,  
205 surface models of the stapes in STL (Standard Tessellation Language) format were obtained  
206 from micro-CT images. The surface models were imported into a commercial software,  
207 RapidForm XOS2 (3D Systems Corp., USA), and a plane, which best fit to the medial surface  
208 of the footplate, was obtained. On the plane, the posterior-anterior direction along the long  
209 axis of the footplate was set as the  $x$ -direction, the inferior-superior direction along the short  
210 axis of the footplate as the  $y$ -direction, and the medial-lateral direction (i.e., the direction  
211 normal to the plane) as the  $z$ -direction. Using the right-hand rule for the right ear (TB1) and  
212 the left-hand rule for the left ear (TB2), the anterior, superior, and lateral directions were set  
213 as the positive  $x$ ,  $y$ , and  $z$  directions. The directions of the long and short axes of the footplate

214 were determined such that the ratio of the length along the short axis to the length along the  
215 long axis was minimized (Sim et al. 2013).

216 While the  $xyz$  directions of the intrinsic frame were determined with surface models of  
217 the stapes, the center of mass of the malleus-incus complex, which was calculated from 3-D  
218 volume data of the malleus-incus complex, was set as the origin of the intrinsic frame. In the  
219 calculation, only the high-density bony parts were considered, and uniform density was  
220 assumed for the high-density parts (Sim et al. 2007, 2013).

221

### 222 **2.3.2 Registration into intrinsic frame**

223 Once the 3-D features of the middle-ear ossicles and the markers reconstructed from  
224 the micro-CT frame were registered into the intrinsic frame, transformation between the LDV  
225 measurement frames and the intrinsic frame (anatomical frame) was obtained, based on the  
226 coordinates of the markers in both frames. For the registration, the 3-D features of the middle-  
227 ear ossicles and the markers in the intrinsic frame were transformed to each of the LDV  
228 measurement frames by rotations and translations, such that the  $XY$  coordinates of the markers  
229 recorded in the LDV measurement frame (see Section 2.2) fit the location of the markers in  
230 the intrinsic frame. Thereby, transformation from the intrinsic frame to the LDV measurement  
231 frame was defined by the rotations and translations performed during the registration. Figure  
232 2a illustrates the 3-D features of the middle-ear ossicles and the markers aligned into the LDV  
233 measurement frame for orientation of TB1.

234 Then, since only the  $XY$  coordinates of the measurement points were recorded in the  
235 LDV measurement frame, identification of the  $Z$  coordinates of the measurement points was  
236 required. The identification of the  $Z$  coordinates of the measurement points was done using a  
237 custom-made ray-tracing algorithm, which is based on the OPCODE collision detection  
238 library (Terdiman 2001) and implemented in Matlab (MathWorks, USA). For each  
239 measurement point, a virtual laser beam was made such that it passed through the  $XY$   
240 coordinates of the measurement point. The virtual laser beam started at a point located on the  
241 side of the LDV unit with a positive  $Z$  coordinate larger than the maximum value of the  
242 surface geometry, and was pointed toward the surface geometry. Then, the coordinates of the  
243 first intersection point between the virtual laser beam and the surface geometry were the  
244 coordinates of the measurement point in the LDV measurement frame (right in Fig. 2b).

245 After the transformation from the intrinsic frame to the LDV measurement frame was  
246 identified including the  $Z$  coordinates of the measurement points in the LDV measurement  
247 frame, it was reversed to obtain the transformation of the measurement points from the LDV

248 measurement to the intrinsic frame. Figure 3 illustrates the measurement points in each of the  
 249 three LDV measurement frames (i.e., three different orientations) and all the corresponding  
 250 points registered in the intrinsic frame (TB1).

251

## 252 2.4. Calculation of the rigid body motion (RBM) components

253 Once all the measurement points on the malleus and the incus are registered to the  
 254 intrinsic frame, the vector  $\mathbf{v}_r$  of the six rigid-body motion components of each of the malleus  
 255 and the incus is related to the velocity vector  $\mathbf{v}_m$  at the point  $m$  on the bone in the intrinsic  
 256 frame by

$$257 \quad \mathbf{v}_m = \mathbf{B}_m \mathbf{v}_r, \quad (1)$$

$$258 \quad \text{with } \mathbf{B}_m = \begin{bmatrix} 1 & 0 & 0 & 0 & z_m & -y_m \\ 0 & 1 & 0 & -z_m & 0 & x_m \\ 0 & 0 & 1 & y_m & -x_m & 0 \end{bmatrix} \text{ and } \mathbf{v}_r = \begin{Bmatrix} \mathbf{v}_o \\ \boldsymbol{\omega} \end{Bmatrix} = \begin{Bmatrix} v_{ox} \\ v_{oy} \\ v_{oz} \\ \omega_x \\ \omega_y \\ \omega_z \end{Bmatrix}.$$

259 where  $\mathbf{v}_o$  and  $\boldsymbol{\omega}$  indicates vectors for the translational velocity at the origin and the rotational  
 260 velocity of the rigid body, and  $(x_m, y_m, z_m)$  are the coordinates of the point  $m$  in the intrinsic  
 261 frame. The velocity vector  $\mathbf{v}_m$  of the point  $m$  in the intrinsic frame is obtained from the  
 262 corresponding velocity vector  $(\mathbf{v}_m)_{\text{MF}}$  in the LDV measurement frame by

$$263 \quad \mathbf{v}_m = \mathbf{A}_{\text{MF} \rightarrow \text{IF}, m} (\mathbf{v}_m)_{\text{MF}}, \quad (2)$$

264 where  $\mathbf{A}_{\text{MF} \rightarrow \text{IF}, m}$  indicates transformation matrix from the LDV measurement frame to the  
 265 intrinsic frame, which is obtained based on methods described in Section 2.3. Combining Eqs.  
 266 (1) and (2),

$$267 \quad (\mathbf{v}_m)_{\text{MF}} = \mathbf{A}_{\text{IF} \rightarrow \text{MF}, m} \mathbf{B}_m \mathbf{v}_r, \quad (3)$$

268 with  $\mathbf{A}_{\text{IF} \rightarrow \text{MF}, m} = \mathbf{A}_{\text{MF} \rightarrow \text{IF}, m}^{-1}$  (transformation matrix from the intrinsic frame into the LDV  
 269 measurement frame). Combining all  $n$  measurement points, Eq. (3) leads to

$$270 \quad \mathbf{v}_{\text{MF}} = \mathbf{C} \mathbf{v}_r, \quad (4)$$

$$271 \quad \text{with } \mathbf{v}_{\text{MF}} = \begin{Bmatrix} (\mathbf{v}_1)_{\text{MF}} \\ (\mathbf{v}_2)_{\text{MF}} \\ \vdots \\ (\mathbf{v}_n)_{\text{MF}} \end{Bmatrix} \text{ and } \mathbf{C} = \begin{Bmatrix} \mathbf{A}_{\text{IF} \rightarrow \text{MF}, 1} \mathbf{B}_1 \\ \mathbf{A}_{\text{IF} \rightarrow \text{MF}, 2} \mathbf{B}_2 \\ \vdots \\ \mathbf{A}_{\text{IF} \rightarrow \text{MF}, n} \mathbf{B}_n \end{Bmatrix}.$$

272 To determine the six rigid-body motion components, at least three non-collinear points are  
 273 needed for each of the malleus and the incus (i.e.,  $n \geq 3$ ). Since the measurements of the  
 274 vibrational motion were performed at 6-8 points on the malleus and 8-10 points on the incus,  
 275 the vector  $\mathbf{v}_r$  of the rigid-body motion components was calculated by the method of least  
 276 squares error as

$$277 \quad \mathbf{v}_r = (\mathbf{C}^T \mathbf{C})^{-1} (\mathbf{C}^T \mathbf{v}_{MF}). \quad (5)$$

278

## 279 2.5. Optimization of the RBM calculations

280 While Eq. (5) allows for an RBM fit based on the velocity data from all measurement  
 281 points (i.e., 6-10 points on each ossicle), in practice, not all the measured data from all  
 282 measurement points are suitable for the RBM calculation due to issues with poor signal-to-  
 283 noise ratio (SNR) of the velocity data or ambiguities in the spatial location of the  
 284 measurement points. In order to provide a deterministic approach to choosing an optimal data  
 285 set by excluding problematic velocity data and points, we designed an automatic selection  
 286 procedure that accounts for time waveform coherence, SNR, and RBM fit accuracy of  
 287 measurement data.

288 The procedure consisted of two stages. In the first stage, the waveform of each  
 289 measurement block was compared to the waveform of all other blocks. Based on this, only  
 290 “good” blocks, defined as having less than 5% average deviation from the rest, were used for  
 291 further processing. Then data were averaged among “good” blocks in the frequency domain,  
 292 and the corresponding SNR was estimated by comparison with noise floor measurements.  
 293 Velocity components with an average SNR of less than 10 dB were excluded from further  
 294 calculations.

295 In the second stage of the automatic selection procedure, a diagram, which is shown in  
 296 Fig. 4, the vector  $\mathbf{v}_r$  of the six rigid-body motion components was calculated, the velocity  
 297 vector  $(\mathbf{v}_m)_{MF}$  of each measurement point was reversely calculated from  $\mathbf{v}_r$  using equation (3),  
 298 and the results were compared with the originally measured velocity components. In the case  
 299 that any reversely calculated velocity component showed a large difference from the  
 300 corresponding measured velocity component, the velocity component was removed and the  
 301 rigid-body motion components were recalculated. The iterations were stopped when the  
 302 difference between the RBM fit and the measured data converged to  $< 3$  dB, or when the  
 303 maximum number of iterations (i.e.,  $N < 10$ ) was reached. For the final data set, the average  
 304 ratio between the final RBM fit and measured data was 1-2 dB.

305

### 306 3. Results

#### 307 3.1 Rigid-body motion (RBM) components of the malleus and the incus

308 Figure 5 represents the rigid body motion (RBM) components of the malleus (solid)  
309 and the incus (dashed), normalized by the ear canal pressure, for the fresh temporal bone  
310 (TB1, Fig. 5a) and frozen temporal bone (TB2, Fig 5b). The results from the two sets of  
311 harmonic signals showed continuity at the border frequency (i.e., at 2 kHz), for both  
312 magnitude and phase

313 Comparison between the translational components of the malleus at the center of mass  
314 of the malleus-incus complex (i.e., origin of the intrinsic frame) shows that, at frequencies  
315 below approximately 3.5 kHz, the  $v_{oy}$  (velocity component in superior direction) and  $v_{oz}$   
316 (velocity component in the median direction) are larger than the  $v_{ox}$  (velocity component to  
317 the anterior direction), for both TBs. This can be explained by the hinged lever motion of the  
318 malleus (Bekesy 1960; Wever and Lawrence 1954), considering some amounts of offset of  
319 the center of mass of the malleus-incus complex from the rotational axis of the hinged motion.  
320 The rotational component  $\omega_x$  (rotation about the posterior-anterior axis) of the malleus, which  
321 corresponds to the hinged motion, is larger than other rotational components at low  
322 frequencies (below 2.5 kHz for TB1 and below 4 kHz for TB2). The rotational component  $\omega_y$   
323 (rotation about the inferior-superior axis) of the malleus becomes relatively large at high  
324 frequencies.

325 In the translational components of the incus at the center of mass of the malleus-incus  
326 complex, the  $v_{oy}$  and  $v_{oz}$  have larger magnitudes than the  $v_{ox}$  at low frequencies (below 2.5  
327 kHz for TB1 and below 1.2 kHz for TB2). The rotational component  $\omega_x$  of the incus has  
328 larger magnitudes than other rotational components below 1.5 kHz, and all the rotational  
329 components have similar magnitudes at higher frequencies, for both TBs.

330 The malleus and the incus show differences in their RBM components for both TBs,  
331 indicating relative motion between the two ossicles. In TB1, the magnitudes and phases of  $v_{oy}$   
332 and  $\omega_x$  are similar in the whole frequency range and below 1.2 kHz, respectively. All other  
333 components showed differences in magnitude and phase. The TB2 also shows similar  
334 magnitudes and phases of  $\omega_x$  up to 1.5 kHz. In TB2, the  $v_{oy}$  and  $\omega_z$  have similar magnitudes  
335 and phases in the entire considered frequency range. In both TBs, the rotational component  $\omega_y$   
336 in the malleus has larger magnitudes than the corresponding component in the incus above 2.5  
337 kHz.

338

#### 339 3.2 Transfer function of the lenticularis relative to the umbo

340 Figure 6 illustrates velocities at the umbo of the malleus and at the lenticular process  
341 of the incus (LPI), normalized by the ear canal pressure, for the fresh temporal bone (TB1, Fig.  
342 6a) and frozen temporal bone (TB2, Fig. 6b). The shaded areas in the figures indicate the  
343 normal ranges (95% confidence interval) of the umbo motion (left upper in Fig. 6a and Fig.  
344 6b), based on measurements of in-vivo (Goode et al. 1996; Huber et al. 2001; Whittemore et  
345 al. 2004) and temporal bones (Goode et al. 1994; Kurokawa et al. 1995; Willi et al. 2002;  
346 Rosowski et al. 2004), and the stapes motion (right upper in Fig. 6a and Fig. 6b), based on the  
347 American Society for Testing and Materials (ASTM) standard (F2504-05, Philadelphia, 2005).

348 Both TBs indicate a predominant component in the medial-lateral direction ( $v_{uz}$  and  $v_{iz}$ )  
349 that is 5-15 dB higher at lower frequencies (i.e.,  $< 2$  kHz) than the other components.  
350 Considering the fact that the rotational component  $\omega_x$  contributes mainly to the translational  
351 component of the medial-lateral direction at the umbo and the lenticular process, such results  
352 are consistent with observations from data in Fig. 5. At the lenticular process of TB1, the  
353 component in the medial-lateral direction still remains larger than other components at higher  
354 frequencies, but the differences were less than  $< 5$  dB above 1.5 kHz. The phase was similar  
355 for the components in the  $x$  and  $y$  directions for the umbo of the malleus and the LPI in TB1.  
356 In TB2, all the three velocity components of the LPI have similar magnitudes above 2 kHz.

## 357 **4. Discussion**

### 358 **4.1. Accuracy of the RBM fit**

359 As described in the Introduction, difficulties in measuring three-dimensional motions  
360 of the malleus–incus complex are caused mainly by limitations in the surgical opening for  
361 access of the laser beams of the 3D LDV system to the malleus and the incus without damage  
362 to the suspensory attachments in the middle ear. Though the superior part of the malleus head  
363 and incus body, the manubrium of the malleus, and the long process of the incus were  
364 exposed by a combined surgical opening of a canal-wall-up mastoidectomy and an  
365 epitympanectomy, the measurements were performed with several different angular positions  
366 of the 3D LDV laser beams to obtain a sufficient number of the measurement points. With  
367 such approaches, identification of the angular positions of the 3D LDV laser beams and  
368 registration of the measurement points to the anatomical intrinsic frame were necessary. This  
369 study describes methodologies to resolve the problems and thus measure the full three-  
370 dimensional motions of the malleus and the incus.

371 In addition, in this study, an algorithm to exclude erroneous data and measurement  
372 points was used (see Section 2.5). In the first stage of the algorithm, data blocks with poor  
373 SNR or waveform conformity were excluded, resulting in the removal of  $< 5$  (out of 30)  
374 blocks of the data, on average for all measurements. In the second stage of the algorithm,  
375 approximately 10-20% of the velocity components were excluded, and the RBM was  
376 recalculated with the remaining components. Figure 7 illustrates the magnitudes of the  
377 measured data (solid) in comparison with the magnitude of the corresponding components  
378 recalculated from the obtained RBM (dashed), for the measurement points on the incus in  
379 TB2. In this example, only the velocity components used for the final RBM calculation were  
380 shown in Fig. 7 (i.e.,  $X$  component at I3, I4, and I7, and  $Y$  component at I5 and I9 were  
381 removed during the optimization procedures, as shown in Fig. 7). The recalculated  
382 components generally show good agreement with the originally measured components.

383

### 384 **4.2. Relative motion at the incudo-malleolar joint**

385 In Fig. 5, while a part of the RBM components, including the rotational component  $\omega_x$ ,  
386 have similar magnitudes, some RBM components show phase and magnitude differences  
387 between the malleus and the incus in specific frequency ranges. However, considering the fact  
388 that the rotational component  $\omega_x$ , which corresponds to the hinged motion (rotation around the  
389 inferior-superior direction) of the malleus and incus, is larger than other rotational  
390 components at nearly all frequencies below 3-4 kHz, the malleus and the incus show smaller

391 relative motions below 1.2 kHz, larger relative motions in the 1.5 – 4.5 kHz range, and again  
392 reduced relative motion above 4.5 kHz. Another interesting observation was that the  
393 rotational component  $\omega_y$  (rotation about the inferior-superior direction) in the malleus has  
394 larger magnitudes than the corresponding component in the incus at higher frequencies above  
395 2.5 kHz. Such relatively large magnitudes of the malleus were predicted by Puria and Steele  
396 (2010), where the rotational motion of the malleus about the inferior-superior direction was  
397 described as a “twisting motion”. From their observation of anatomy of the eardrum, malleus,  
398 and the incudo-malleal joint (IMJ), they predicted that the “twisting motion” would be large at  
399 high frequencies in large mammals such as human and cat, and the large “twisting motion” of  
400 the malleus would be transferred to the incus with reduced magnitudes via the mobile IMJ in  
401 the large mammals. Both components,  $\omega_x$  and  $\omega_y$ , show comparable magnitudes at high  
402 frequencies, indicating a complex combination of hinged and twisting motions.

403 The frozen bone (TB2) shows smaller relative motions between the malleus and the  
404 incus than the fresh bone (TB1), for all the RBM components, indicating lower mobility of  
405 the IMJ in the frozen temporal bone. However, only one fresh and one frozen temporal bones  
406 were used in this study, and more samples will be needed to confirm the possible difference  
407 between fresh and frozen conditions of the temporal bones. In addition, it has been known that  
408 there exist large amounts of individual variance in ossicular motion across samples. As shown  
409 in Fig. 6 (shaded areas), individual variance in the velocities at the umbo of the malleus and at  
410 the lenticular process of the incus can be as large as 15 dB through the frequency range  
411 considered in this study.

412

### 413 **4.3. Transmission loss in the malleus-incus complex**

414 Figure 8 illustrates the ratios of the velocity at the LPI to the velocity at the umbo,  
415 which are shown in Fig. 6, for the velocity component  $v_z$  (i.e.,  $v_{iz}/v_{uz}$ ). While the frozen and  
416 fresh temporal bones showed large differences in each of the umbo velocity and the LPI  
417 velocity (Fig. 6), the magnitude ratio and phase difference between the umbo velocity and the  
418 LPI velocity in z-direction were very similar for the bones of the two different conditions  
419 (within <3dB on average across frequencies). Since the LPI is in close proximity to the input  
420 of the incudo-stapedial joint (ISJ), and since previous studies (Huber et al. 2003; Peacock et al.  
421 2015; Allan et al. 2013) indicate low relative motion across the ISJ, the LPI motion can be  
422 assumed to be representative of the motion of the stapes head. Based on that, the velocity  
423 component  $v_{iz}$  of the LPI can be considered as the piston-like motion of the stapes. In both  
424 TBs, the velocity component in the direction of the piston-like motion is attenuated, through

425 the malleus-incus complex, by less than 5 dB below 1.8 kHz, and by more than 10 dB above 2  
426 kHz. The attenuation is explained by the observation that the incus has smaller magnitudes of  
427 the hinged rotational motion than the malleus at high frequencies (see the rotational  
428 component  $\omega_x$  in Fig. 5). Assuming that the motion component  $v_{iz}$  at the lenticular process is  
429 representative of the piston-like motion of the stapes, previous works supports the attenuation  
430 at high frequencies.

431 As the reduction of the hinged rotational motion through the malleus and the incus is  
432 caused by the mobility of the IMJ, immobilization of the IMJ is supposed to increase sound  
433 transmission through the middle ear. In a study by Willi (2003), transmission through the  
434 malleus-incus complex could be increased at high frequencies above 3 kHz by immobilizing  
435 the IMJ. Offergeld et al. (2007) also demonstrated that the amplitude of the stapes motion is  
436 increased in the frequency range of 1.2-5 kHz with immobilization of the IMJ. Recently,  
437 Gerig et al. (2015) showed that the piston-like motion of the stapes with the immobilized IMJ  
438 is increased by 5-8 dB above 2 kHz compared to the corresponding motion with the mobile  
439 IMJ. The reason why the IMJ is mobile even with reduction of the middle-ear transmission  
440 has not been revealed.

441 Additionally, the relative phase difference between the umbo and LPI, with a  
442 maximum of 70deg at 2 kHz, suggests a frequency-dependent group delay of approximately  
443 100 $\mu$ s, which is consistent with a middle-ear group delay of 134 $\mu$ s (including the tympanic  
444 membrane and ossicles) reported by O'Connor and Puria (2006) and while accounting for  
445 transmission delays across the tympanic membrane of approximately 25-40 $\mu$ s (O'Connor and  
446 Puria 2008; Dobrev et al. 2014).

447

## 448 5. Conclusion

449 This work demonstrated methodologies to quantify the full six degrees-of-freedom of  
450 the rigid body motion of the malleus-incus complex (MIC). The results indicate that under  
451 physiologically relevant levels of acoustical stimulation, the hinged rotational motion is  
452 dominant at frequencies below 1.5 kHz, but the motion of the malleus and incus becomes  
453 complex as other motion components increase their significance at higher frequencies. While  
454 the malleus and the incus behave like one rigid body with little relative motion below 1.5 kHz,  
455 the relative motion between the malleus and the incus gets larger at higher frequencies. The  
456 MIC attenuates the hinged rotational motion at frequencies above 2 kHz, and the incus has  
457 smaller rotational motion about the inferior-superior axis than the malleus above 2 kHz.

458 Future work, involving more samples, should include the quantification and analysis  
459 of all motion components for the complete description of the behavior of the MIC under  
460 physiologically relevant acoustic excitation and its effect on the middle-ear function.

ACCEPTED MANUSCRIPT

461 **References**

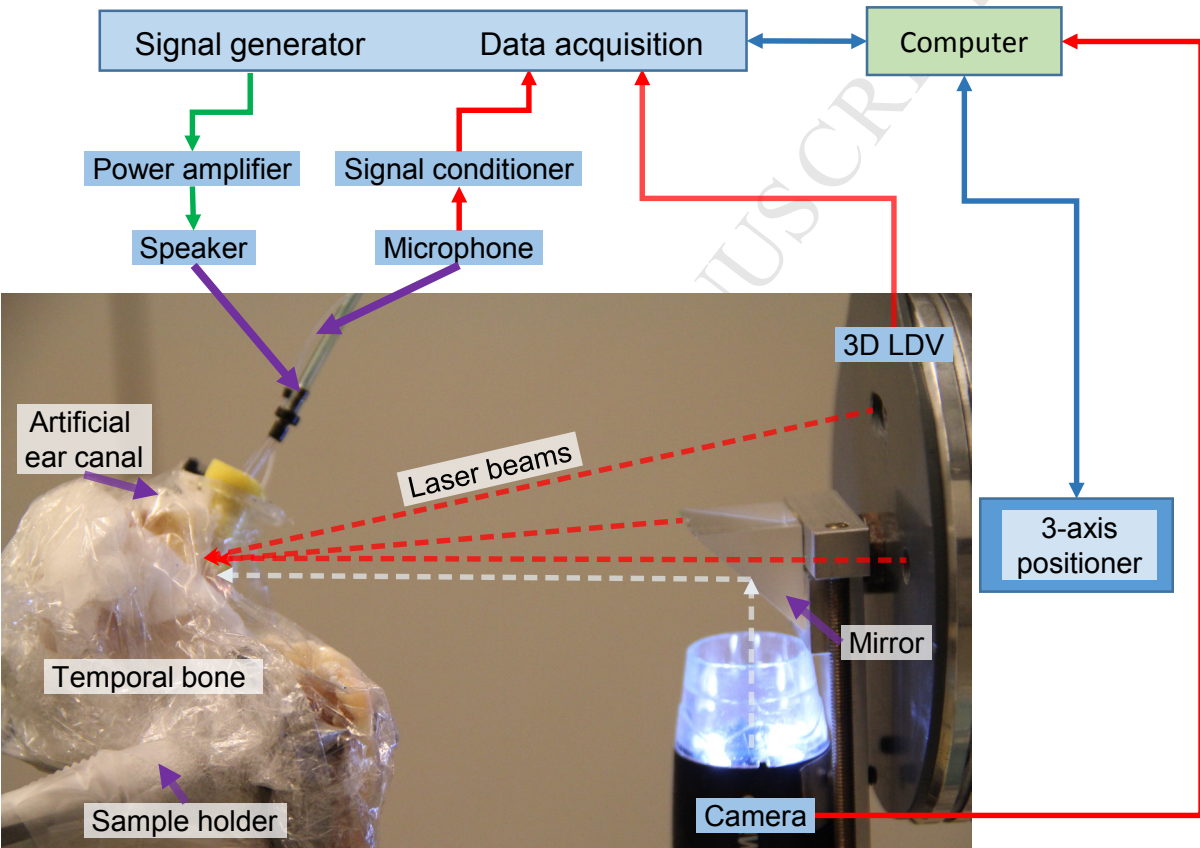
- 462 Alian, W., Majdalawieh, O., Kiefte, M., Ejnell, H., Bance, M., 2013. The Effect of Increased  
463 Stiffness of the Incudostapedial Joint on the Transmission of Air-Conducted Sound by the  
464 Human Middle Ear. *Otology & Neurotology*, 34(8), 1503-1509.
- 465 Decraemer W.F., Khanna S.M., and Funnell W.R.J., 1994. A method for determining three-  
466 dimensional vibration in the ear. *Hear. Res.* 77(1-2), 19-37.
- 467 Decraemer W.F., Khanna S.M., and Funnell W.R.J., 1999. Vibrations at a fine grid of points  
468 on the cat tympanic membrane measured with a heterodyne interferometer. In EOS/SPIE  
469 International Symposia on Industrial Lasers and Inspection, Conference on Biomedical Laser  
470 and Metrology and Applications.
- 471 Decraemer W.F., de La Rochefoucauld O., Dong W., Khanna S.M., Dirckx J.J.J., and Olson  
472 E.S., 2007. Scala vestibuli pressure and three-dimensional stapes velocity measured in direct  
473 succession in gerbil. *JASA* 121, 2774–2791.
- 474 Decraemer, W., de La Rochefoucauld, O., Funnell, W., Olson, E.S., 2014. Three-Dimensional  
475 Vibration of the Malleus and Incus in the Living Gerbil, *JARO*, 15, 483-510.
- 476 Dobrev, I., Furlong, C., Cheng, J. T., Rosowski, J. J., 2014. Full-field transient vibrometry of  
477 the human tympanic membrane by local phase correlation and high-speed holography.  
478 *Journal of biomedical optics*, 19(9), 096001-096001.
- 479 Ihrle, S., Eiber, A., Eberhard, P., 2015. Experimental investigation of the three dimensional  
480 vibration of a small lightweight object. *Journal of Sound and Vibration* 334: 108-119.
- 481 Gatto, M., Peeters, B., Coppotelli, G., 2010. Flexible shaker excitation signals for improved  
482 FRF estimation and non-linearity assessment. In Proceedings of the ISMA 2010 International  
483 Conference on Noise and Vibration Engineering.
- 484 Gerig, R., Ihrle, S., Rösli, C., Dalbert, A., Dobrev, I., Pfiffner, F., Eiber, A., Huber A.M.,  
485 Sim J.H., 2015. Contribution of the incudo-malleolar joint to middle-ear sound transmission.  
486 Accepted in *Hear. Res.*

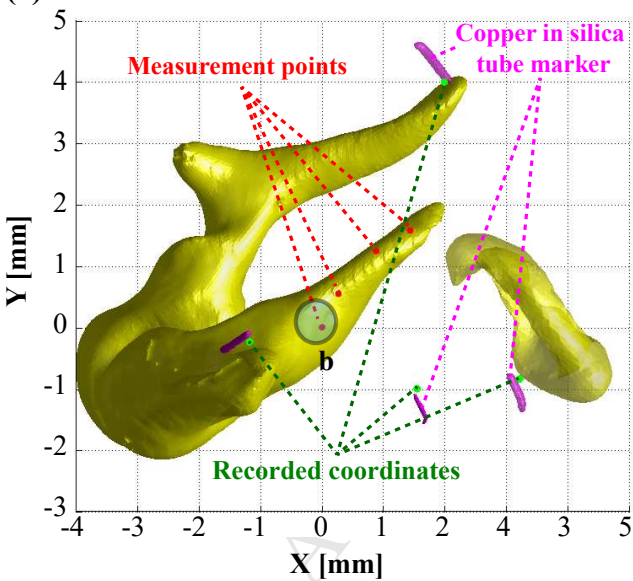
- 487 Goode, R. L., Killion, M., Nakamura, K., Nishihara, S., 1994. New knowledge about the  
488 function of the human middle ear: development of an improved analog model. *Otology &*  
489 *Neurotology*, 15(2), 145-154.
- 490 Goode, R. L., Ball, G., Nishihara, S., & Nakamura, K., 1996. Laser Doppler Vibrometer  
491 (LDV) a new clinical tool for the otologist. *Otology & Neurotology*, 17(6), 813-822.
- 492 Hato, N., Stenfelt, S., Goode, R.L., 2003. Three-dimensional stapes footplate motion in  
493 human temporal bones. *Audiology & Neuro-Otology*, 8, 140-152.
- 494 Huber, A. M., Schwab, C., Linder, T., Stoeckli, S. J., Ferrazzini, M., Dillier, N., Fisch, U.,  
495 2001. Evaluation of eardrum laser Doppler interferometry as a diagnostic tool. *The*  
496 *Laryngoscope*, 111(3), 501-507.
- 497 Huber, A. M., Ma, P., Felix, H., Linder, T., 2003. Stapes Prosthesis Attachment:  
498 The Effect of Crimping on Sound Transfer in Otosclerosis Surgery. *Laryngoscope*,  
499 113, 853–858.
- 500 Kurokawa, H., Goode, R., 1995. Sound pressure gain produced by the human middle ear. *Am.*  
501 *J. Otology*, 113: 349-355.
- 502 Lauxmann, M., Eiber, A., Heckler, C., Ihrle, S., Chatzimichalis, M., Huber, A.M., Sim, J.H.,  
503 2012. In-plane motions of the stapes in human ears. *JASA*, 132(5), 3280-3291.
- 504 O'Connor, K. N., Puria, S., 2006. Middle ear cavity and ear canal pressure-driven stapes  
505 velocity responses in human cadaveric temporal bones. *JASA*, 120(3), 1517-1528.
- 506 O'Connor, K. N., Puria S., 2008. Middle-ear circuit model parameters based on a population  
507 of human ears. *JASA*, 123(1), 197.
- 508 Peacock, J., Dirckx, J., von Unge, M., 2015. Towards quantitative diagnosis of ossicular  
509 fixation: Measurement of stapes fixations using magnetically driven ossicles in human  
510 temporal bones. *Acta oto-laryngologica*, (0), 1-6.
- 511 Puria, S., 2003. Measurements of human middle ear forward and reverse acoustics:  
512 implications for otoacoustic emissions. *JASA*, 113(5): 2773-2789.

- 513 Puria, S., Sim, J. H., Shin M., Steele, C. R., 2007. A gear in the middle ear. *The 30th*  
514 *Association for Research in Otolaryngology Winter Research Meeting, Denver, Colorado.*
- 515 Puria, S., and Steele, C.R., 2010. Tympanic membrane and malleus-incus-complex co-  
516 adaptations for high-frequency hearing in mammals. *Hearing Research*, 263, 183-190.
- 517 Rosowski, J. J., Mehta, R.P., Merchant, S.N., 2004. Diagnostic utility of laser-doppler  
518 vibrometry in conductive hearing loss with normal tympanic membrane. *Otol. Neurotol.*,  
519 25(3): 323–332.
- 520 Sim, J. H., Puria, S., Steele, C. R., 2004. Three-dimensional measurement and analysis of the  
521 isolated malleus-incus complex. In K. Gyo & H. Wada (Eds.), *The 3rd International*  
522 *Symposium on Middle Ear Mechanics in Research and Otology*, (pp. 61–67). Singapore:  
523 World Scientific.
- 524 Sim, J. H., Puria, S., 2008. Soft tissue morphometry of the malleus-incus complex from  
525 micro-CT imaging. *JARO*, 9: 5-21.
- 526 Sim, J. H., Puria, S., Steele, C.R., 2007. Calculation of the inertial properties of the malleus-  
527 incus complex from micro-CT imaging. *Journal of Mechanics of Materials and Structures*, 2  
528 (8): 1515-1524.
- 529 Sim, J. H., Puria, S., 2009. An electro-magnetic force and moment motor: Application to  
530 small-scale biological structures. *IEEE Sensors Journal*, 9: 1924-1932.
- 531 Sim, J. H., Chatzimichalis, M., Lauxmann, M., Rösli, C., Eiber, A., Huber, A.M., 2010a.  
532 Complex stapes motions in human ears. *JARO*, 11(3): 329-341.
- 533 Sim, J. H., Chatzimichalis, M., Lauxmann, M., Rösli, C., Eiber, A., Huber, A.M., 2010b.  
534 Errors in measuring three-dimensional motions of the stapes using a laser Doppler vibrometer  
535 system. *Hear. Res.*, 270: 4-14.
- 536 Sim, J. H., Chatzimichalis, M., Rösli, C., Laske, R.D., and Huber, A.M., 2012. Objective  
537 assessment of stapedotomy surgery from round window motion measurement. *Ear & Hearing*,  
538 33(5): 24-31.
- 539 Terdiman, P., 2001. Memory-optimized bounding-volume hierarchies.  
540 <http://www.codercorner.com/Opcode.htm>

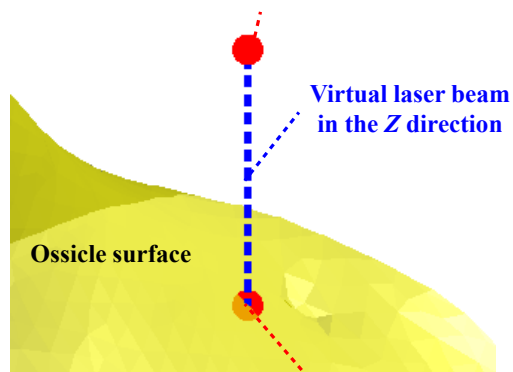
- 541 Whittemore, K. R., Merchant, S. N., Poon, B. B., Rosowski, J. J., 2004. A normative study of  
542 tympanic membrane motion in humans using a laser Doppler vibrometer (LDV). *Hearing*  
543 *Research*, 187(1), 85-104.
- 544 Willi, U. B., Ferrazzini, M. A., Huber, A. M., 2002. The incudo-malleolar joint and sound  
545 transmission losses. *Hearing research*, 174(1), 32-44.

546 **Figure Captions**547 **Fig 1.** Schematic illustration of the measurement setup.548 **Fig 2.** 3-D features of the middle-ear ossicles and the markers aligned into the LDV  
549 measurement frame (a) and illustration of the ray-tracing with virtual laser beams for  
550 identification of the Z coordinates of the measurement points (b), for the orientation of TB1.551 **Fig 3.** Measurement points in the three LDV measurement frames with three different  
552 orientations (a-c) and all the corresponding points registered in the intrinsic frame (d), for  
553 TB1.554 **Fig 4.** Validation of calculation of rigid body motion (RBM) components.555 **Fig 5.** Rigid body motion (RBM) components of the malleus (solid) and the incus (dashed),  
556 normalized by the ear canal pressure, (a) for fresh temporal bone (TB1) and (b) for frozen  
557 temporal bone (TB2).558 **Fig 6.** Velocities at the umbo of the malleus and at the lenticular process of the incus (LPI),  
559 normalized by the ear canal pressure, (a) for fresh temporal bone (TB1) and (b) for frozen  
560 temporal bone (TB2). The shaded areas, outlined with dashed lines, in the figures indicate the  
561 normal ranges (95% confidence interval) of the umbo motion (light gray), based on literature,  
562 and the stapes motion (dark gray), based on ASTM standard.563 **Fig 7.** Magnitudes of the measured data (solid) in comparison with the magnitude of the  
564 corresponding components recalculated from the obtained RMB (dashed), for the  
565 measurement points on the incus in the TB2.566 **Fig 8.** Ratios of the velocity at the lenticular process of the incus (LPI) to the velocity at the  
567 umbo for the component in the z direction (lateral-medial direction).



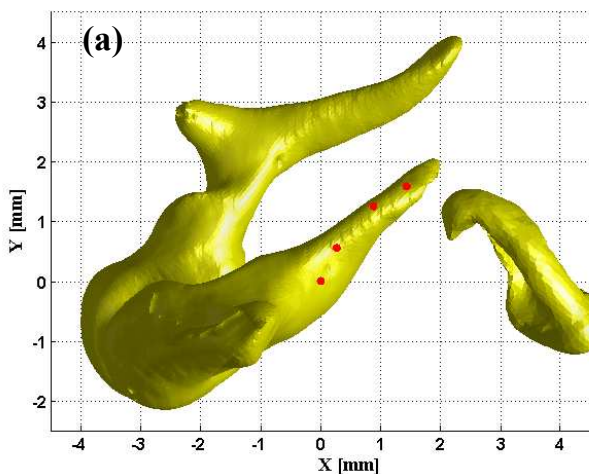
**(a) LDV Measurement Frame: TB1 Orientation 1****(b)**

Starting point of the virtual laser beam with XY coordinates of the measurement point

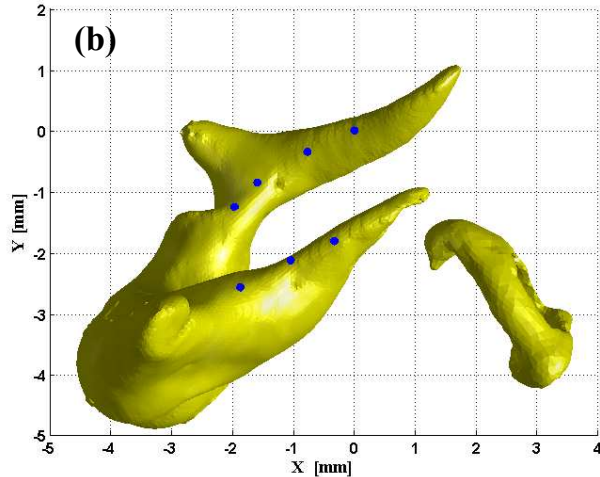


Obtained measurement point as intersection between the virtual laser beam and surface

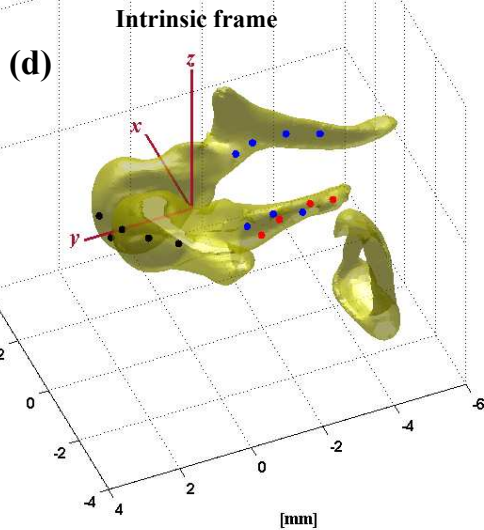
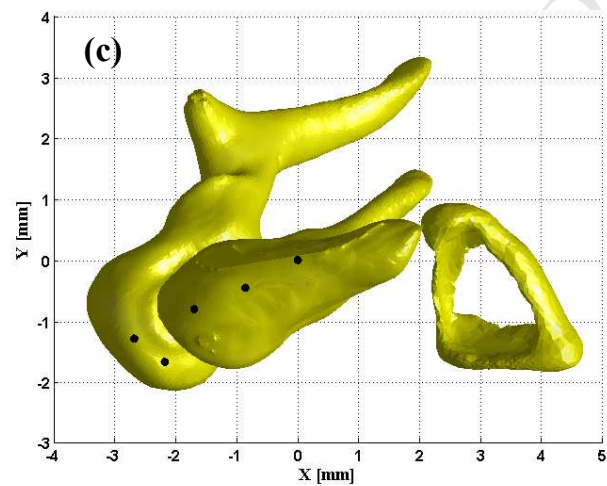
LDV Measurement Frame: TB1 Orientation 1



LDV Measurement Frame: TB1 Orientation 2



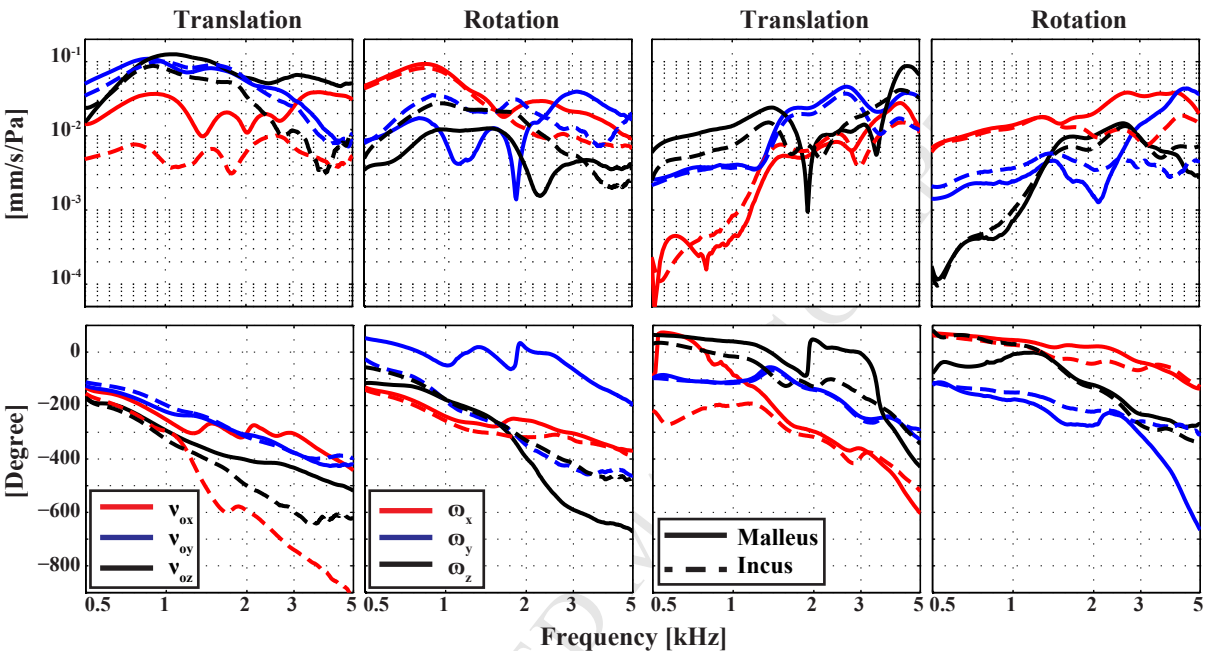
LDV Measurement Frame: TB1 Orientation 3

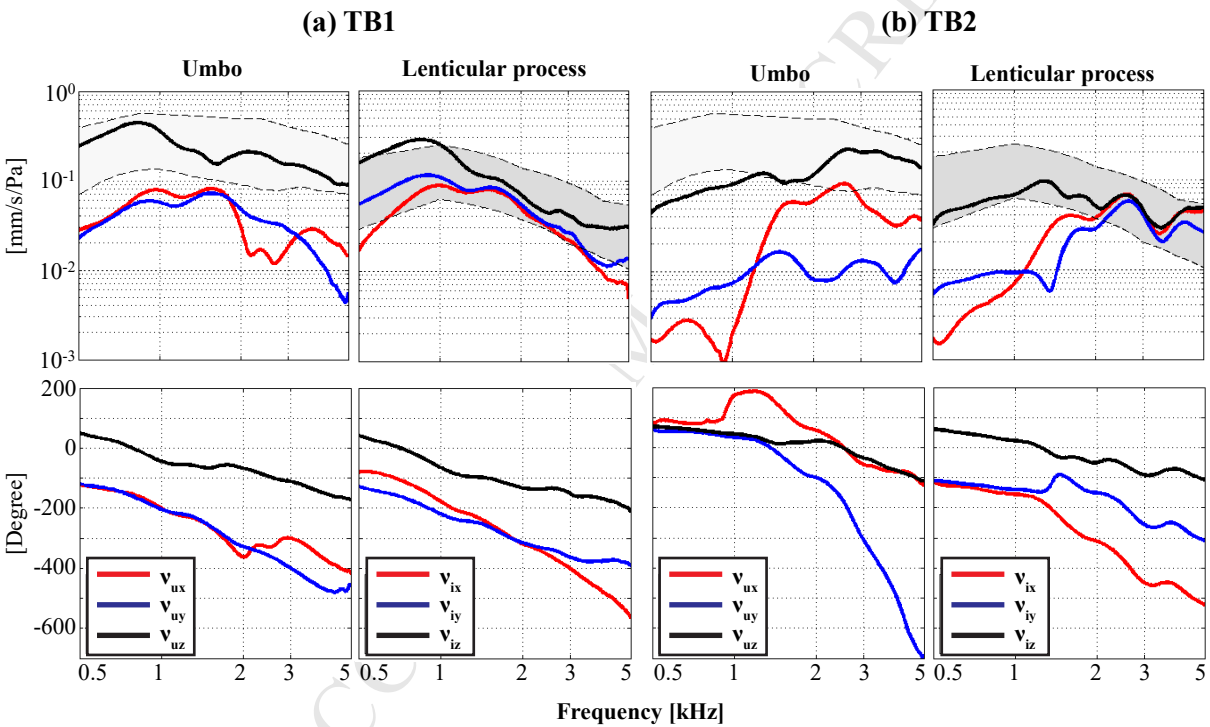


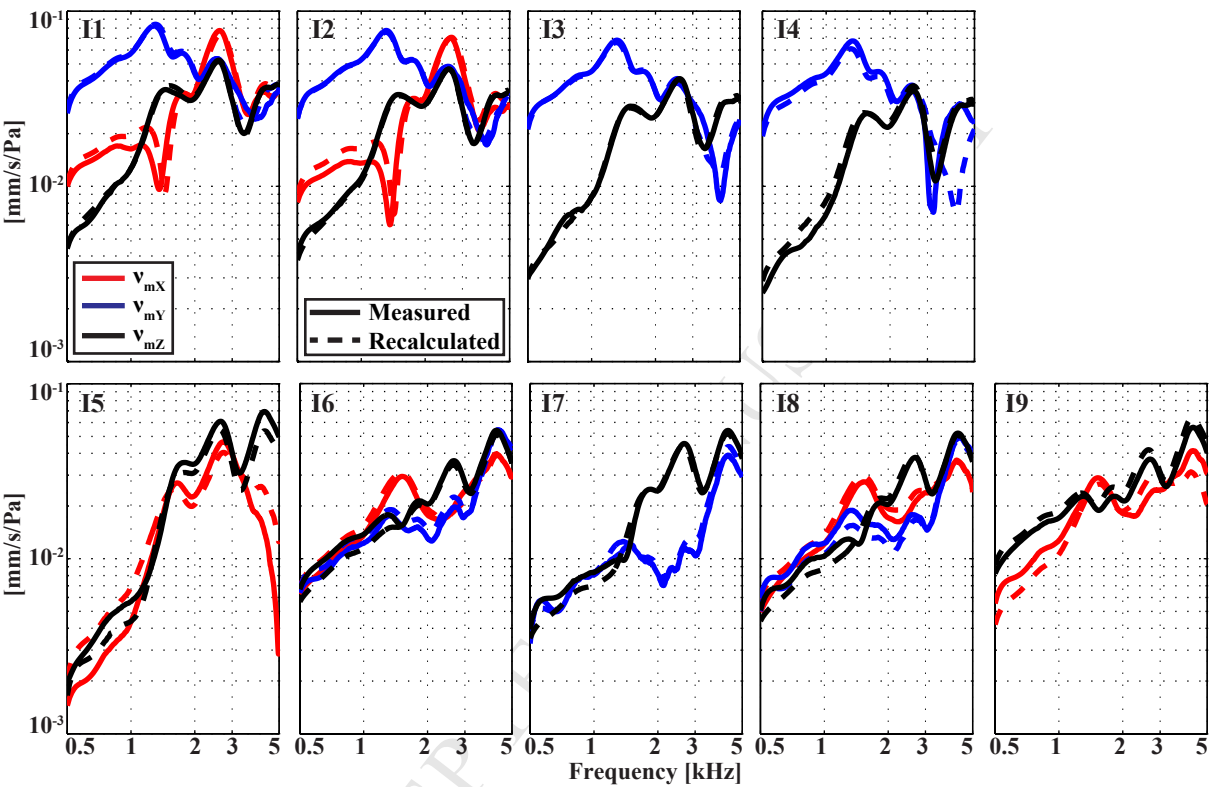


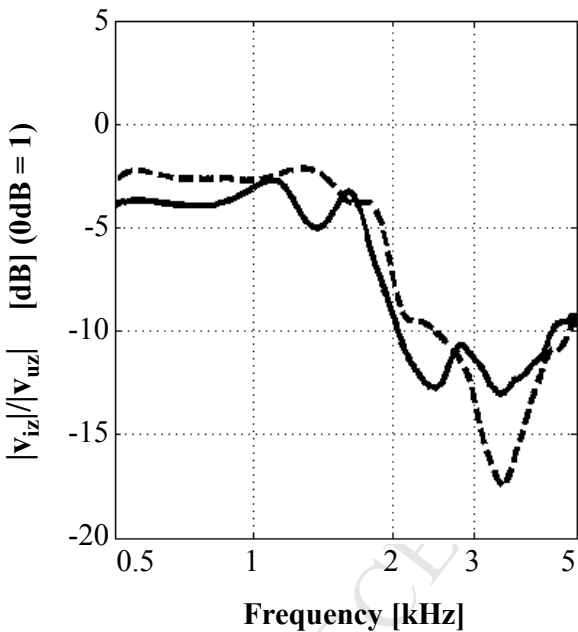
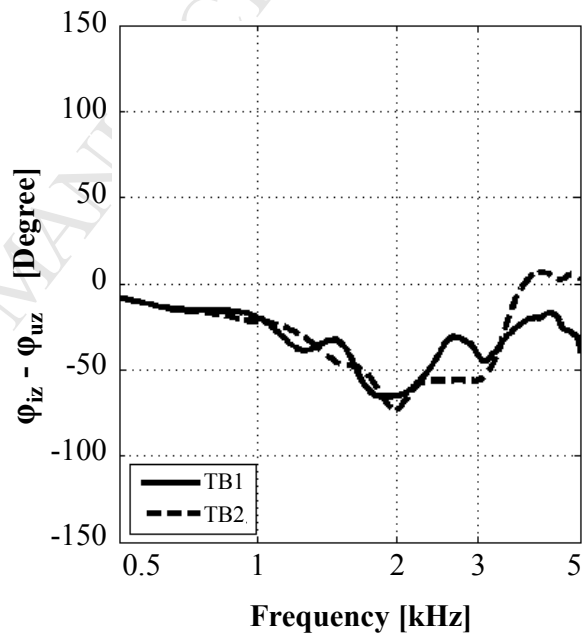
(a) TB1

(b) TB2







**Magnitude Ratio****Phase Difference**

**Research Highlights**

- Demonstrated methodologies to quantify the full six degrees-of-freedom of the rigid body motion of the malleus-incus complex (MIC).
- The MIC motion is defined by a predominant hinged rotational component below 1.5 kHz.
- The rotation about the inferior-superior direction, or “twisting motion”, in the malleus has larger magnitudes than the corresponding component in the incus above 3 kHz.
- While the magnitude of the transfer function of the MIC decreases with frequency, its spatio-temporal complexity increases significantly